Modeling of a mixed-load fluvio-deltaic system

N. Geleynse,[1] J. E. A. Storms,[1] M. J. F. Stive,[2] H. R. A. Jagers,[3] and D. J. R. Walstra[2,3]

Received 3 December 2009; revised 1 February 2010; accepted 3 February 2010; published 4 March 2010.

[1] Present-day observations and classical classification schemes of alluvial deltas address feeder channel dynamics and multiple sediment fractions. However, high-resolution physics-based mathematical models have not been applied to address formation of both fluvio-deltaic links (channels) and nodes (diffluences and confluences), and their stratigraphy. Here, we present a simulated delta system under riverine forcing that shows striking similarity to its counterparts recognized in field and laboratory studies. These findings include distinct shifts in river planimetrical mode and altimetry, deltaic mouth bar and distributary formation, lateral fining in migrating-meander bend axes and fining-upward patterns in passive delta-plain distributaries. **Citation:** Geleynse, N., J. E. A. Storms, M. J. F. Stive, H. R. A. Jagers, and D. J. R. Walstra (2010), Modeling of a mixed-load fluvio-deltaic system, *Geophys. Res. Lett.*, *37*, L05402, doi:10.1029/2009GL042000.

1. Introduction

[2] Considerable attention has been devoted to investigation of measures to sustain activity along deltaic shorelines. However, no generic model framework is available to systematically study physical river-delta (trans)formation.

[3] From field studies regarding fluvial distributary systems [e.g., *Roberts et al.*, 1980], three distinct aspects can be inferred: (1) the sediment flux towards downstream basins to form a distributary network can be significantly driven by high-magnitude flood events, (2) the river channel does not merely function as a gateway for its own building blocks, but continuously alters to take on particular planimetrical and altimetrical modes at certain discrete time-points, and (3) the sedimentary characteristics of hinterland, river-channel bed and banks, and receiving basin are of importance to the build-up of deltaic sedimentary records in lacustrine or marine basins. These aspects may sound logical to the thoughtful observer, however, present-day deltaic shoreline models typically do not address them in combined form, though consideration and reinterpretation of real-world observations and classical mathematical descriptions led *Dade* [2000] to point at, and call for, further investigations regarding the issues listed above.

[4] Fundamentally, the constitution of fluvial distributary systems is governed by [*Jerolmack and Swenson*, 2007] (1) local bar deposition at the shoreline inducing flow bifurcation, hence channel lengthening, and (2) regional relocation of the feeder channel (belt), induced by local or regional factors. However, dynamics of (self-similar components of) a deltaic network (subdelta, delta lobe) may at some time-point, for some time span, be characterized by dominance of either of the two processes. Using detrended fluctuation analysis, *Seybold et al.* [2009] found dynamics of a burst-prograding delta based on their reduced complexity model to have a characteristic timescale, which separates a highly correlated regime for small timescales from a less correlated one at larger timescales. The former corresponded to consistent delta growth via gradual shoreline deposition while the latter corresponded to rapid change, associated with large-scale channel avulsions resulting in channel formation and subaqueous dominated deposition. Also, rather than focusing on allogenic forcing variability, experimental shoreline migration under steady and sole riverine forcing was assessed to exhibit pulses, associated with a channelization instability releasing sediment from a non-cohesive fan delta surface, preceded by, and alternating with, deposition-dominant sheet flow conditions, to give rise to cyclic sedimentation packages [*Kim and Jerolmack*, 2008].

[5] The origin and stability of nodes of fluvial distributary systems (particularly diffluences) have been extensively studied [e.g., *Kleinhans et al.*, 2008], however, an integrated quantitative representation of both nodes and links, prime constituents of deltaic networks, is still in its incipient stage [*Edmonds and Slingerland*, 2009]. Moreover, coupling of vertical and horizontal displacements of these geomorphic entities to their internal sedimentary composition allows for river system characterization [*Jerolmack and Mohrig*, 2007].

[6] Here, we show results from a high-resolution physics-based numerical model of a river-delta system that addresses mixed-load transport conditions, river-bed and bank stratigraphy, and which relocates the upstream boundary condition to account for a channel that is not necessarily "in equilibrium" with existing flow conditions. As such, we relax the presently limited representation of the interface of riverine land and semi-unconfined basin waters, and demonstrate the need for detailed field and laboratory data that address alluvial deltas and their feeder systems, concurrently.

2. Computer Model Description

[7] Adopting the view of movement of sediment particles as a phenomenon of advection-diffusion in the water flow and assuming relatively low concentrations of relatively fine sediment (lower than c.0.1 by volume and smaller than c.0.001 m, respectively), one arrives at a coupled model of clear water with sediment transport. Herein, the isopycnal fluid flow field is computed by discretization of the well-known unsteady depth-averaged shallow-water equations on a rectangular staggered finite difference grid and solved by means of an alternate direction implicit time-integration

[1]Department of Geotechnology, Delft University of Technology, Delft, Netherlands.
[2]Hydraulic Engineering, Delft University of Technology, Delft, Netherlands.
[3]Deltares, Delft, Netherlands.

0094-8276/10/2009GL042000$05.00

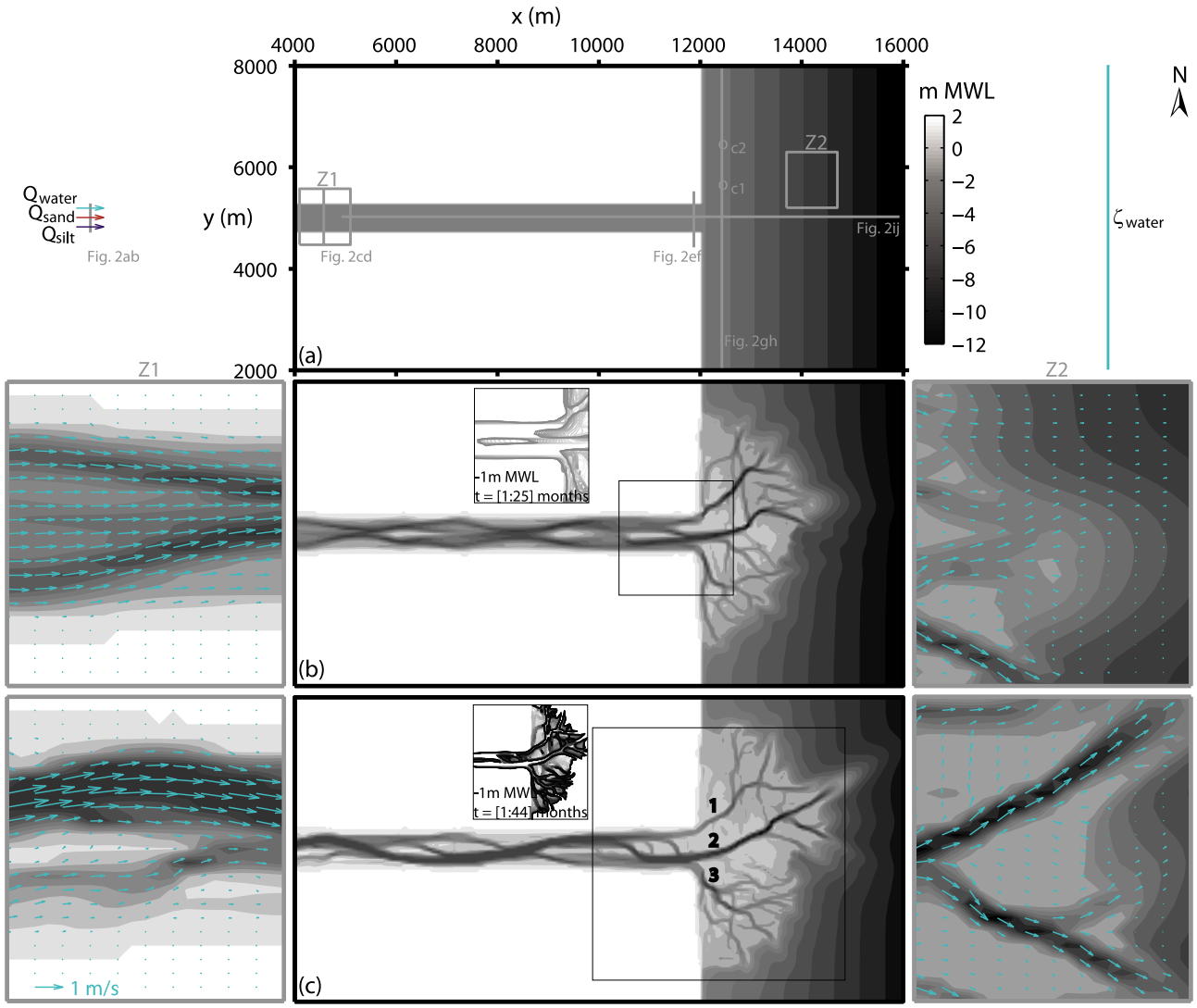

Model Parameter	Value	Unit
Manning's n	0.03	s $m^{-1/3}$
Coefficient representing diffusion and dispersion of helical flow intensity	1.0	m^2 s^{-1}
Horizontal turbulent diffusivity of fluid momentum	1.0	m^2 s^{-1}
Sand diameter	0.000125	m
Sand dry density	1600	kg m^{-3}
Silt fall velocity	0.0015	m s^{-1}
Silt dry density	500	kg m^{-3}
Horizontal turbulent diffusivity of sediment	1.0	m^2 s^{-1}
Coefficient representing probability of deposited silt to adhere to bed	1	
Erodibility coefficient silt	0.0001	kg m^{-2} s^{-1}
Critical shear stress for silt erosion	0.5	N m^{-2}

Figure 1. Simulated (trans)formation of a river-delta system. (a) initial configuration; (b) multiple bar and distributary network formation (t = 25 months); (c) attainment of a dominant meandering mode (see also Figures 2c and 2d) and organisation of distributary channels on delta plain (t = 45 months). Boundary types, locations of profiles and cores of Figure 2 are indicated. Boxes (Z1 and Z2) in Figure 1a refer to zoom of development of part of the (left) river and (right) basin, respectively. Simulated depth-averaged flow field is thinned in streamwise direction. Insets in Figures 1b and 1c show upstream growth of bars until t = 25 months and stacked view of distributary dynamics, respectively.

method. To account for spiral flow, correction terms are included in the fluid momentum equations; the effective radius of streamline curvature is derived from the spiral flow intensity, which is obtained from an advection-diffusion formulation [*Deltares*, 2008]. At closed boundaries (dry river banks or bars emerging above a critical flow depth; herein set at 0.1 m), a free-slip condition is assumed. The bed shear stresses are related to components of the depth-averaged velocity vector by Chézy's relation. To meet the requirement of Courant numbers for fluid advection to be below unity, for reasons of accuracy, a time step of 15 s is chosen. Horizontal grid cell dimensions are 50 m.

[8] In need for isolation of the natural deltaic shoreline system, upstream drainage basin dynamics are collapsed to a

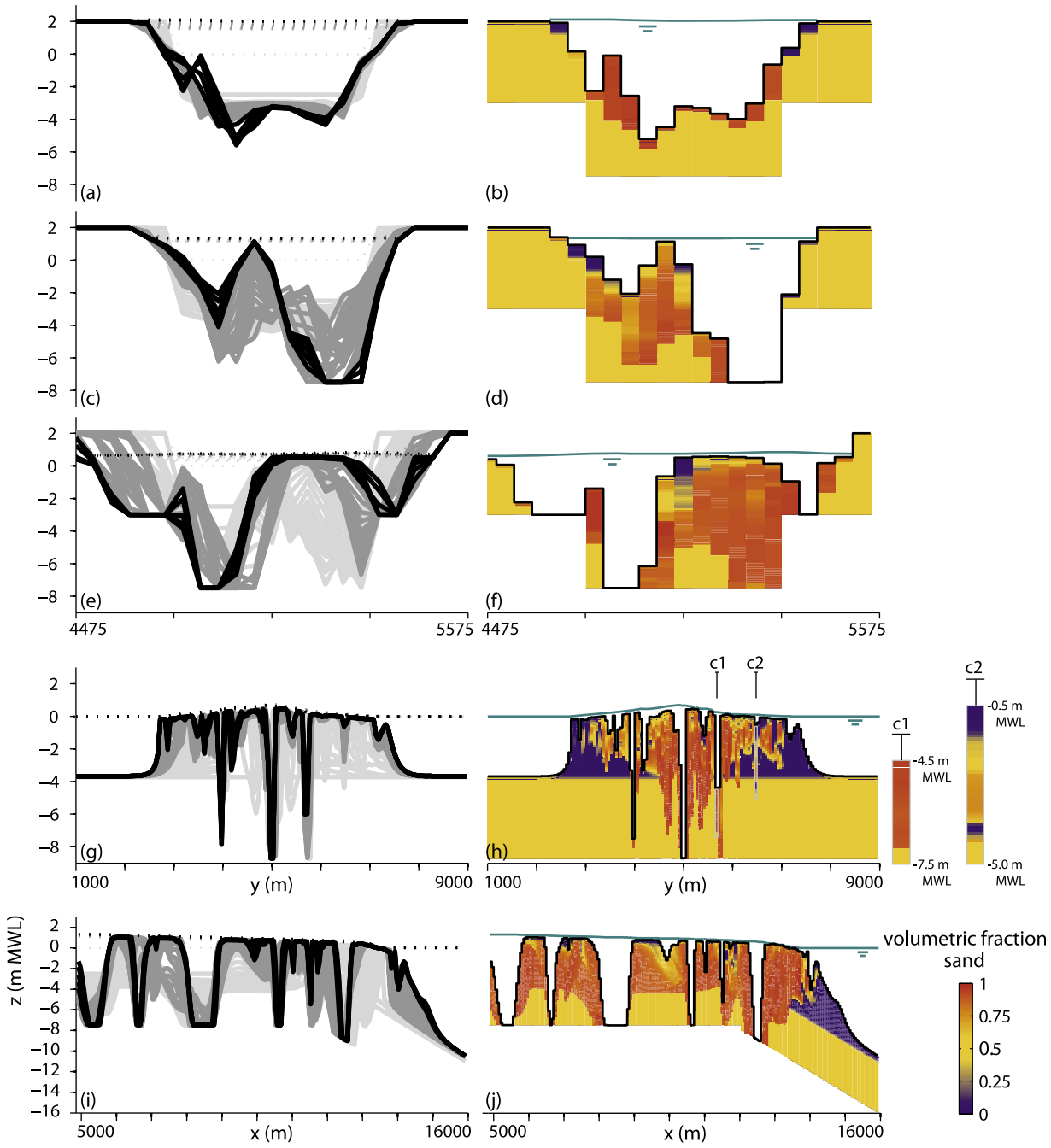

Figure 2. (left) Simulated spanwise (Figures 2a, 2c, 2e, and 2g) and streamwise (Figure 2i) bed- (solid lines) and water level (dotted lines) dynamics. Light-gray, dark-gray and black lines indicate channel developments for first (600 days), second (600 days) and third period (150 days), respectively, with a display temporal resolution of 30 days. (right) Corresponding simulated stratigraphy at final time-point. In Figure 2h, zoom of virtual cores display an active and passive distributary, that in earlier phases of delta progradation issued from same lower-order parent channel.

morphologically inactive line boundary (fixed cross-section, 2.5 m deep, 550 m wide) through which water ($Q_{water}(t)_{|x=0}$ = 2000 m^3s^{-1}), fine sand ($Q_{sand}(t)_{|x=0} = f(z_b(x, y, t))$; Neumann condition) and coarse silt ($Q_{silt}(t)_{|x=0}$ = 40 mg l^{-1}) are discharged (where t, x, y, z_b denote time, rectangular Cartesian coordinates, bed level relative to mean water level, MWL). Initial geometry, horizontal boundaries and relevant parameter settings are depicted in Figure 1. In the present schematization, downstream forcings are left out of consideration. In view of (1) these simplifications, (2) a mathematical problem that is to be well-posed and (3) Froude numbers being well below unity, a time-invariant water level ($\zeta(t)_{|x=20,000}$ = 0 m MWL) is prescribed at the offshore boundary.

[9] The transport of fine sand is modeled algebraically, according to the Engelund-Hansen formulation [e.g., *Garcia*, 2006]. Among many other available formulae, each having their pros and cons [*Garcia*, 2006], effects of longitudinal and transverse bed slopes are accounted for, following the widely-applied Bagnold-Ikeda expressions [e.g.,

Garcia, 2006]. A depth-averaged advection-diffusion formula is used to compute transport of coarse silt. Herein, the erosion rate (modeled as a linear function of excess shear stress) and deposition rate follow from the well-known Krone-Mehta-Partheniades formulations [e.g., *Garcia*, 2006]. For an overview on the approximation of the concentration profile, used to determine the transfer of suspended and bed sediment via so-called source and sink terms, refer to *Deltares* [2008]. The transport equation is discretized with a finite volume approximation.

[10] The bed is schematized following a multi-layer concept [e.g., *Garcia*, 2006]. Here, we use a transport layer

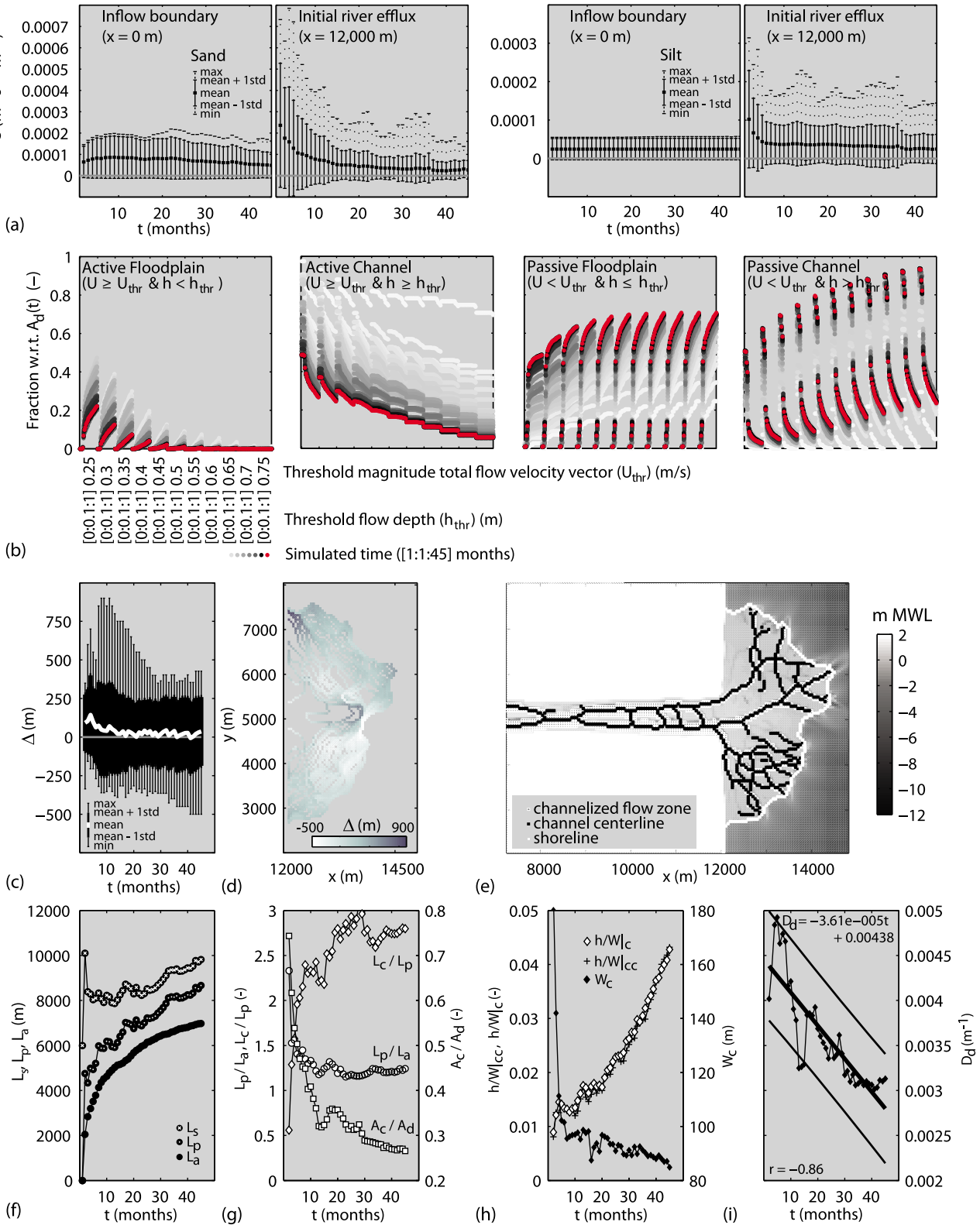

Figure 3

of fixed height in space and time (0.2 m) and a maximum number of 75 bookkeeping layers (each 0.1 m thick) to track sedimentary composition. As an initial condition, the entire spatial domain is characterized by a fully-mixed 5 m-sediment layer. The basement is assumed unerodible; sediment fluxes are reduced if the immobile substrate is reached (supply-limited condition). The quantity of sand and silt available at the bed transport layer is updated for each (half) 'hydrodynamical' time step by means of bookkeeping for the control volume of each computational cell. Before morphological computations are performed, a spin-up interval of 3600 s is used for introductory adaptation of the flow field. Under the assumption of timescales for relaxation of non-Newtonian fluids being well beyond those for Newtonian fluids, the potential bed level change is linearly upscaled, to extend the time horizon of classical morphodynamical models [*Roelvink*, 2006] (cf. the Deborah number by *Reiner* [1964]). Here, a factor of 60 is used. To allow for erosion of river banks and emergent bars, sediment (per fraction) which is eroded from an active grid cell is (uniformly) replenished from its adjacent inactive cells, which, thence may be activated. If a certain sediment fraction is not (sufficiently) present in the neighboring cells, the eroded volume is replenished with a volume that is made up of (enriched with) the other sediment fraction. For an elaborate treatment of the bed level procedure, as well as of the drying and wetting of (in)active cells, refer to *Deltares* [2008].

3. Linked River-Delta Representation and Discussion

[11] Starting with a straight non-sloping channel emptying into a linearly-sloping basin (Figure 1a), multiple bars (transverse oscillation mode = 2–3) develop in the confined river valley (Figure 1b), that widens, the degree of which increases at the river orifice (Figures 2a, 2c, and 2e). The latter is caused by stream bifurcation at the efflux, preceded by deposition of sediment resulting from divergence of the transport field to form a mouth bar [*Edmonds and Slingerland*, 2007]. Erodibility of lateral boundaries of rivers is of fundamental importance to occurrence and dynamics of natural forms such as bars and meanders [*Seminara*, 2006]. Here, alternate bar formation in the upstream part of the semi-confined river zone is initiated by a bank-line instability, entailing local width variations that, in turn, promote central bar formation (Figure 1b). This process is controlled by the large initial channel aspect ratio (220) and relative high degree of non-linearity of the Engelund-Hansen transport law (5), under conditions of easily erodible fines (low critical erosional shear stress; 0.5 Nm^{-2}) and overall sand-dominated fluxes (Figure 3a), hence negative damping lengths. Observed downstream response can also be inferred from linear analyses [e.g., *Crosato*, 2008, and references therein]. Under identical system forcing, but assuming river banks to be inerodible results in persistence of the initial straight planform (here not shown). In both cases, however, the bed configuration of the lower river is also influenced by downstream deposition at the efflux, which induces a morphodynamic feedback. This is manifested through the growth of the initial mouth bar at its upstream tail over hundreds of metres (Figure 1b inset) following rapid shoreline progradation during first few time steps (Figure 3f), and later becoming dissected by small transverse streams (traceable by upward and transverse fining patterns; Figures 2e and 2f) which, in turn, link the different feeder channels (Figure 1c). Upstream growth of mouth bars has also been recognized from progradation of Atchafalaya and Wax deltas, Burdekin delta and Lena delta [*Olariu and Bhattacharya*, 2006] and in experiments, under conditions of low Froude numbers ($\ll$1) [*Hoyal and Sheets*, 2009].

[12] Prior to the first flow bifurcation at the efflux, sandy subaqueous levees form along the margins of the jet, with fines being dispersed farther basinward (Figure 2g–2j). Flow diverges over the crest of the developing mouth bar focusing sediment towards the subaqueous levees, which breach. Resultantly, high-angle bifurcates (up to 90° w.r.t. river-basin axis) form. However, being typically unstable [e.g., *Federici and Paola*, 2003] these are incapable of progressive capture of the main stem flow, as the flow subsequently concentrates at the centerline, dissecting the mouth bar. Under high, but decreasing riverine sediment supply (Figure 3a), the delta than progrades three channel widths into deeper ambient water before the longitudinal slope becomes too small to transport sediment any farther. Consequently, the afore-mentioned bifurcates are reactivated after 6 simulated months leading to the initial stage of delta

Figure 3. (a) Time series of sediment transport rate for both fractions at inflow boundary and river efflux. Its distribution over the cross-section of fixed width (1200 m) is indicated. (b) Fraction of delta area (A_d; see Figure 3e) occupied by four basic geomorphic entities, defined according to different combinations of thresholded flow depth ($h = \zeta - z_b$) and magnitude of depth-averaged total flow velocity vector (U), and sensitivity of classification to chosen thresholds (h_{thr} and U_{thr}). (c) Time series of distribution of local shoreline variability (Δ) along the perturbed shoreline (L_p), defined as the distance of each perturbed shoreline cell to its nearest cell on a semi-circle (same grid resolution) of length L_a, bounding an area of equal magnitude (A_d). (d) Corresponding locations (stacked shorelines). (e) Example of the output (t = 45 months) of an image processing algorithm, that identifies shoreline position, channelized flow zones (active channel class of Figure 3b with h_{thr} = 1 m, U_{thr} =.25 m/s) and their centerlines (skeletons). For simplicity, delta area (A_d) is defined as the zone seaward of x = 12,000 m and bounded by classified shoreline positions. (f) Time series of L_p, L_a and total shoreline length (L_s), the latter measured between fixed positions at the initial unperturbed shoreline; deviation between L_s and L_p indicates lateral dynamics of the delta surface. The relative large value for L_s at t = 2 corresponds to strong looping of the perturbed shoreline associated with deposition of bars at the lateral sides of the initial bifurcates with limited shoreline-attached deposition. (g) Time series of dimensionless parameters, where L_c is summed distributary length measured along the extracted centerlines of (e) ($x \geq$ 12,000 m), A_c is channelized flow area of A_d. (h) Time series of equivalent (mean) channel width ($W_c = A_c/L_c$) and depth-to-width ratio, calculated from the mean flow depth along the channel centerlines (subscript cc) and for A_c. (i) Time series of drainage density ($D_d = L_c/A_d$) with least-squares-fit and confidence bounds.

progradation being mainly oriented parallel to the undisturbed shoreline (cf. *Seybold et al.* [2009] for larger timescales). Herewith associated, maximum local shoreline roughness increases (Figures 3c and 3d), while drainage density (Figure 3i) and channelized flow portion of the delta surface area (Figure 3g) decrease, the degree of which depends on the actual definition of "a channel" (Figures 3b and 3e).

[13] First-order developments during subsequent phases of delta formation comprise an organising distributary network (Figure 1c), being overall characterized by (1) a decreasing number (here not explicitly shown) of (2) more persistent channels (Figures 3b and 3g–3i; stronger ability to differentiate between active channel and passive floodplain classes, negative correlation between dimensionless shoreline extension and dimensionless channelized flow area, increasing mean channel aspect ratio and decreasing drainage density, respectively), (3) that rejoin less frequently [cf. *Martin et al.*, 2009] and (4) have a common progressive tendency to extend more radially-uniformly (corroborating one-dimensional assumption of *Parker and Sequeiros* [2006] for effective description of delta-front propagation), but (5) inducing local shoreline roughening (Figures 3c and 3d), as well as (6) exhibiting distinct sorting patterns (Figures 2h and 2j). Note that this channel organisation implies an apparent lack of necessity to include vegetational strength [e.g., *Tal and Paola*, 2007]. In addition, higher-order variability can be assessed in time series of the governing variables as the system tends asymptotically towards a steady final configuration (Figures 3f–3i). Most notable is the relative increase of dimensionless channelized flow area at the interval t = 14–18 months (Figure 3g), resulting from partial capture of discharge from the central distributary by multiple, less persistent traverse channels. This leads to the assessed increase of shoreline length being more evenly distributed, hence maximum shoreline roughness does not increase (Figure 3c). Accordingly, the temporal increase of L_c/L_p for this interval (Figure 3g) is the result of an increasing number of channels rather than increasing lengths of existing channels.

[14] *Kim and Jerolmack* [2008] and *Hoyal and Sheets* [2009] highlighted downstream control of autogenic behaviour of noncohesive and cohesive experimental deltas under supercritical and subcritical flow conditions. While morphodynamic feedback as a consequence of downstream deposition is important in the present numerical model as well, upstream control to delta lobe shifting is also assessed here. After 41 simulated months, downstream migration of a bar into the throat of channel 1 (Figure 1c) almost results in fixation of the northern delta lobe, coinciding with flooding of southern parts of the delta plain (off channel 3; Figure 1c). However, lateral shift of this channel (channel 1; Figures 2e and 2f) at the final time-step prevents full abandonment. We hypothesize that assessed downstream meander migration (here not shown, but note the simulated classical fining patterns across its axis in Figures 2c and 2d), combined with upstream discharge fluctuations will further direct water and sediment distribution over the different branches, thereby determining stability of individual nodes of the network. Corresponding timescales may vary considerably, with nearly balanced bifurcations developing at a much lower rate than unbalanced bifurcations, explaining observed differences in avulsion duration [*Kleinhans et al.*, 2008]. Concerning characteristic timescales of system response, our simulated river-delta of order kilometer develops within a time span of the order of a year, while natural fluvial distributary systems typically develop on timescales of decades, centuries or even longer, as determined by many factors [e.g., *Syvitski and Milliman*, 2007]. However, effective morphological timescales are for many field cases not deciphered. Detailed studies of *Roberts et al.* [1980] regarding (trans)formation of Atchafalaya deltas are a noteworthy exception, clearly linking scouring of relative unconsolidated lake- and channel infill along considerable stretches of the lower river during river floods to rapid growth of delta mouth bars. Hence, the present simulation can be regarded as a compressed time series of high-discharge events (cf. the common usage of an "intermittency factor" in long-term morphodynamical modelling), it must also be realized that morphological preconditioning is of fundamental importance [*Lane and Richards*, 1997]. Here, the initial state of the feeder system is that of a wide, shallow, easily erodible sand-silt bed; future investigations must focus on the role of this initial schematization in terms of both geometry and internal sedimentary composition, in direct correspondence to upstream water and sediment supply and downstream conditions, as apparent from the present investigation.

[15] **Acknowledgments.** Q. Ye, P. Cowell, and referees are gratefully acknowledged for stimulating discussion. Funding was provided by Water Research Center Delft, Deltares, and StatoilHydro (contract 4501725117).

References

Crosato, A. (2008), Analysis and modelling of river meandering, Ph.D. thesis, 251 pp., Delft Univ. of Technol., Delft, Netherlands.

Dade, W. B. (2000), Grain size, sediment transport and alluvial channel pattern, *Geomorphology*, *35*(1–2), 119–126.

Deltares (2008), *Delft3D-Flow Manual 3.14.5661*, 232 pp., Delft, Netherlands. (Available at http://delftsoftware.wldelft.nl/)

Edmonds, D. A., and R. L. Slingerland (2007), Mechanics of river mouth bar formation: Implications for the morphodynamics of delta distributary networks, *J. Geophys. Res.*, *112*, F02034, doi:10.1029/2006JF000574.

Edmonds, D. A., and R. L. Slingerland (2009), Significant effect of sediment cohesion on delta morphology, *Nat. Geosci.*, *3*, 105–109, doi:10.1038/ngeo730.

Federici, B., and C. Paola (2003), Dynamics of channel bifurcations in noncohesive sediments, *Water Resour. Res.*, *39*(6), 1162, doi:10.1029/2002WR001434.

Garcia, M. E. A. (2006), *Sedimentation Engineering: Processes, Measurements, Modeling, and Practice*, vol. 110, Am. Soc. of Civ. Eng., Reston, Va.

Hoyal, D. C. J. D., and B. A. Sheets (2009), Morphodynamic evolution of experimental cohesive deltas, *J. Geophys. Res.*, *114*, F02009, doi:10.1029/2007JF000882.

Jerolmack, D. J., and D. Mohrig (2007), Conditions for branching in depositional rivers, *Geology*, *35*(5), 463–466, doi:10.1130/G23308A.1.

Jerolmack, D. J., and J. B. Swenson (2007), Scaling relationships and evolution of distributary networks on wave-influenced deltas, *Geophys. Res. Lett.*, *34*, L23402, doi:10.1029/2007GL031823.

Kim, W., and D. J. Jerolmack (2008), The pulse of calm fan deltas, *J. Geol.*, *116*(4), 315–330.

Kleinhans, M. G., H. R. A. Jagers, E. Mosselman, and C. J. Sloff (2008), Bifurcation dynamics and avulsion duration in meandering rivers by one-dimensional and three-dimensional models, *Water Resour. Res.*, *44*, W08454, doi:10.1029/2007WR005912.

Lane, S. N., and K. S. Richards (1997), Linking river channel form and process: Time, Space and Causality revisited, *Earth Surf. Processes Landforms*, *22*, 249–260.

Martin, J., B. Sheets, C. Paola, and D. Hoyal (2009), Influence of steady base-level rise on channel mobility, shoreline migration, and scaling properties of a cohesive experimental delta, *J. Geophys. Res.*, *114*, F03017, doi:10.1029/2008JF001142.

Olariu, C., and J. P. Bhattacharya (2006), Terminal distributary channels and delta front architecture of river-dominated delta systems, *J. Sediment. Res.*, *76*(2), 212–233.

Parker, G., and O. Sequeiros (2006), Large scale river morphodynamics: Application to the Mississippi Delta, in *River Flow 2006: Proceedings of the International Conference on Fluvial Hydraulics*, edited by R. M. L. Ferreira et al., pp. 3–11, Taylor and Francis, London.

Reiner, M. (1964), The Deborah number, *Phys. Today*, *17*(1), 62.

Roberts, H. H., R. D. Adams, and R. H. W. Cunningham (1980), Evolution of the sand-dominated subaerial phase, Atch-afalaya delta, Louisiana, *AAPG Bull.*, *64*, 264–279.

Roelvink, J. A. (2006), Coastal morphodynamic evolution techniques, *Coastal Eng.*, *53*(2–3), 277–287.

Seminara, G. (2006), Meanders, *J. Fluid Mech.*, *554*, 271–297.

Seybold, H. J., P. Molnar, H. M. Singer, J. S. Andrade Jr., H. J. Herrmann, and W. Kinzelbach (2009), Simulation of birdfoot delta formation with application to the Mississippi Delta, *J. Geophys. Res.*, *114*, F03012, doi:10.1029/2009JF001248.

Syvitski, J. P. M., and J. D. Milliman (2007), Geology, geography, and humans battle for dominance over the delivery of fluvial sediment to the coastal ocean, *J. Geol.*, *115*, 1–19, doi:10.1086/509246.

Tal, M., and C. Paola (2007), Dynamic single-thread channels maintained by the interaction of flow and vegetation, *Geology*, *35*(4), 347–350, doi:10.1130/G23260A.1.

N. Geleynse and J. E. A. Storms, Department of Geotechnology, Delft University of Technology, 1, Stevinweg, NL-2628 CN Delft, Netherlands. (n.geleynse@tudelft.nl)

H. R. A. Jagers, Deltares, 185, Rotterdamseweg, PO Box 177, NL-2600 MH Delft, Netherlands.

M. J. F. Stive and D. J. R. Walstra, Hydraulic Engineering, Delft University of Technology, 1, Stevinweg, NL-2628 CN Delft, Netherlands.